VERIZONA PUBLISHER
Publishing Your Ideas

www.verizonaonlinepublishing.com
Vol: 2, Issue: 1

Journal of Nanoscience with Advanced Technology

Hierarchical Bismutite-gold Core-shell Nanostructures for Surface Enhanced Raman Spectroscopy

Hong Hu[1,2] and Xinyi Zhang[*1]

[1]School of Chemistry, Monash University, Clayton, VIC 3800, Australia

[2]Department of Applied Chemistry, Nanjing Polytechnic Institute, Nanjing 210048, China.

***Corresponding author:** Xinyi Zhang, PhD, Lecturer, School of Chemistry, Monash University, Clayton, VIC 3800, Australia; Tel: 61399024619; Fax: 61399044559; Email: xinyi.zhang@monash.edu

Article Type: Research, **Submission Date**: 13 October 2016, **Accepted Date:** 31 October 2016, **Published Date:** 22 February 2017.

Citation: Hong Hu and Xinyi Zhang (2017) Hierarchical Bismutite-gold Core-shell Nanostructures for Surface Enhanced Raman Spectroscopy. J Nanosci Adv Tech 2(1): 1-4. doi: https://doi.org/10.24218/jnat.2017.20.

Abstract

Synthesis and characterization of highly sensitive SERS-active substrates is of significant interest for the detection of chemical and biological molecules. Using the preparative technique described here we have developed a new SERS substrate based on a hierarchical bismutite/gold core-shell nanostructure, prepared by depositing a layer of gold nanoparticles on the three-dimensional bismutite nanostructures. Such core-shell nanostructure has been utilized as a novel surface-enhanced Raman spectroscopy platform for ultrasensitive detection of aromatic molecules with a detect limit below 1nM.

Keywords: Self-assembly, Bismutite, Nanostructures, Surface-enhanced Raman spectroscopy.

Introduction

Surface-enhanced Raman scattering (SERS)-based signal amplification and detection techniques have been widely investigated for non-destructive and label-free detection of organic and biological molecules. The SERS enhancements generally depend on the nanoscale characteristics of the plasmonic metallic substrates, such as surface morphology [1-2], and size and aggregated state of nanoparticles. A number of attempts have been made to fabricate high-performance SERS substrates, for examples, engraving periodical nanosphere arrays by lithography [3], self-organizations of nanoparticles in the solutions [4] and nanoporous substrates[5-7]. However, SERS-based molecule detection strategies have not been practically useful because there is no straight forward method to synthesize and characterize highly sensitive SERS-active nanostructures with sufficiently high yield and efficiency.

Inspired by biomineralization processes, self-assembly of nanocrystals into complex or three-dimensional (3D) nanostructures has received much attention particularly for applications in energy and biomedical fields [8-9]. The ability to produce various nanocrystals through simple synthetic strategies has opened up the possibility of assembling them into tailored superstructures. Our interest in designing functional nanostructures has inspired us to explore the possibility of self-assembling ternary nanocrystals with controlled morphologies into 3D hierarchical nanostructures and thereby their associated properties. Ternary bismutite ($(BiO)_2CO_3$, BSC) has long been used for medicinal purposes, as an anti-inflammatory, antibacterial, and antacid [10-11]. Further, there is considerable interest in BSC nanomaterials given their utility in photocatalytic applications [12-16]. Here, we present a facile approach for the synthesis of 3D BSC hierarchical nanostructures. We find that the formation and growth of 3D BSC nanostructures through the self-assembly of BSC nanocrystals, which strongly depend on a synergistic effect between hydroxide and citrate ions. 3D BSC- gold nanoparticles core-shell nanostructures have been prepared by depositing a layer of gold nanoparticles on the BSC nanostructure. We demonstrate that the 3D BSC/Au nanoparticle core-shell nanostructures can act as an ultra-sensitive surface-enhanced Raman scattering (SERS) sensor.

Experimental Section

BSC crystals were prepared via hydrothermal reaction of bismuth nitrate, and urea. In a typical synthesis of BSC square nanoplates, 30 ml solutions containing 10 mmol of bismuth nitrate ($Bi(NO_3)_3$) and 2.5 g urea were loaded into a Teflon autoclave after 30 min magnetic stirring. The NaOH concentration was adjusted to 0.1 M. The components of the solution for the synthesis of BSC octagonal sheets, round disks and hierarchical nanostructures are the same as above except for the addition of sodium citrate ($Na_3C_6H_5O_7$) and the change in the NaOH concentrations. The autoclave was sealed and maintained at 180°C for 6 h and then allowed to cool naturally to room temperature. After rinsing with distilled water and absolute ethanol to remove possible residues, the products were finally dried at 60°C and collected. All chemical reagents were of analytical grade and used without further purification.

The 3D BSC/Au nanoparticles core-shell spheres were fabricated by using the 3D BSC nanostructures prepared at 40 mmol $Na_3C_6H_5O_7$ and 0.01 M NaOH. The BSC samples were activated

in a solution containing 1 g/liter $PdCl_2$ and 5 g/liter HCl for 2 h, and then 5 mg of BSC samples were added to 2 ml of the following deposition solution: 12 g/liter $HAuCl_4$, 10 g/liter N_2H_4. H_2O, 160 g/liter Na_2SO_3, 5 g/liter EDTA, 30 g/liter K_2HPO_4, 0.5 g/liter $CoSO_4$; PH 9.0. The growth and deposition of Au nanoparticles on the 3D BSC samples was carried out with a magnetic agitation at 60 °C for 4h. The obtained BSC/Au nanoparticles core-shell sphere sample was subsequently rinsed with distilled water. Then, the samples were exposed to UV-ozone at an oxygen flow rate of 3 L min^{-1} for 10 min. After the UV-ozone treatment, the samples were immersed in 2 mL of different concentrations of benzenethiol inethanol solution and left for 12 h, upon which the samples were rinsed with ethanol and then dried. For comparison, a commercial Klarite SERS substrate was exposed to UV ozone and benzenethiol under the same conditions as the BSC/Au nanoparticles core-shell spheresamples prior to the SERS measurements.

The structure and morphology of the BSC crystals were investigated using an X-ray diffractometer (XRD, PW1140/90) with Cu Kα radiation (25 mA and 40 kV), a scanning electron microscope (SEM, JEOL JSM-7001F). The absorbance of the dye solutions was recorded using an agilent Cary 60 ultaviolet–visible spectrometer. The Raman spectrawere recorded using a Confocal micro-Raman System (Renishaw RM 2000) equipped with a near-IR diode laser at a wavelength of 782 nm (laser power: 1.15 mW and laser spot size: 1 μ m). All of the Raman spectra were collected by fine-focusing a 50 × microscope was 10 s.

Results and Discussions

The morphologies of the BSC crystals obtained under various conditions were observed by scanning electron microscopy (SEM). Three-dimensional BSC nanostructures with controlled crystalline morphology, orientation and surface architectures were fabricated through the self-assembly of BSC nanocrystals. Figure 1 shows the SEM images of the 3D BSC nanostructures formed through assembly of various BSC nanocrystals. Figures 1a and 1b shows 3D BSC nanostructures prepared in the presence of 20 mmol sodium citrate and 0.01 M NaOH. The sphere-like 3D BSC nanostructures are composed of packed square nanoplates with 200-400 nm long edges and 30-40 nm thicknesses. Figures 1c and 1d shows the 3D BSC nanostructures prepared in the presence of 30 mmol sodium citrate and 0.01 M NaOH. The open-hole BSC nanostructures are composed of packed round nanosheets with 400–800 nm sizes and 40–60 nm thicknesses. Figures 1e and 1f shows the 3D BSC nanostructures prepared in the presence of 40 mmol sodium citrate and 0.01M NaOH. The 3D BSC nanostructures are composed of close packed nanodisks with diameters of 100–500 nm and thicknesses of 20–40 nm, respectively. The X-ray diffraction patterns of the 3D BSC nanostructures are shown in Figure 2. In comparison with BSC nano- and microcrystals, the {001} peaks are less pronouncedbecause fewer {001} facets are exposed due to the stacking and angles.

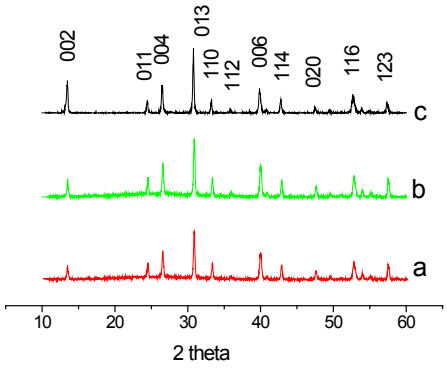

Figure 2: XRD patterns of the BSC nanostructures obtained under different conditions: (**a**) 20mmol $Na_3C_6H_5O_7$ 0.01MNaOH, (**b**) 30 mmol $Na_3C_6H_5O_7$ 0.01M NaOH, (**c**) 40 mmol $Na_3C_6H_5O_7$ 0.01M NaOH

Citrate ion is the principle reason for the assembly of BSC nanocrystals since the 3D BSC nanostructures can not be obtained in the absence of citrate ions. The adsorption of citrate ions on the {001} surface of BSC nanocrystals may balance the interactions among the BSC nanocrystals, binding the BSC nanocrystals into 3D nanostructures. From the above analyses, it can be concluded that citrate and hydroxide ions are the two crucial factors for morphology control of BSC crystals. Their importance depends on their respective concentrations. BSC plates, sheets, or disks occur at lower citrate ion concentration

Figure 3 shows the SEM images of the BSC/ Au NPs spheres produced. The 3D BSC nanostructures were covered by well dispersed Au NPs of diameters in the range 40-80 nm, and the

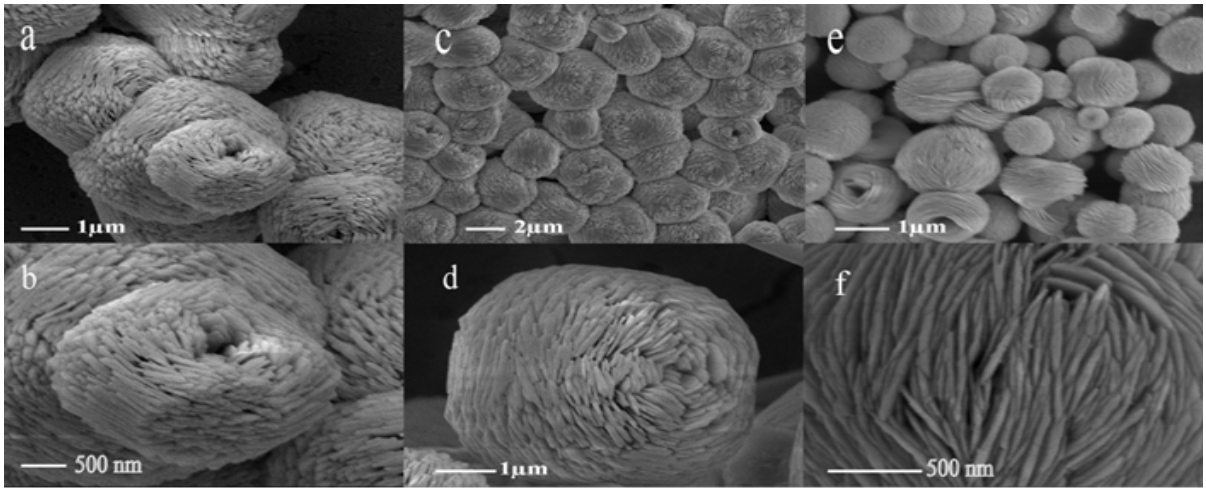

Figure 1: SEM images of the 3D BSC nanostructures obtained under different conditions: (**a,b**) 20 mmol $Na_3C_6H_5O_7$ 0.01M NaOH, (**c,d**) 30 mmol $Na_3C_6H_5O_7$ 0.01M NaOH, (**e,f**) 40 mmol $Na_3C_6H_5O_7$ 0.01M NaOH

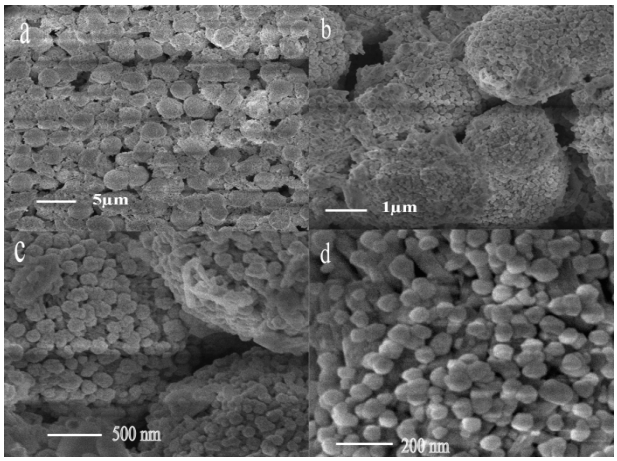

Figure 3: SEM images of 3D BSC/Au nanoparticles spheres at different magnifications

resulting core-shell spheres retain the shape and size of the 3D BSC nanostuctures.

The SERS performance of the 3D BSC/Au NP core-shell spheres was investigated by using benzenethiol as a model analyte. Figure 4 shows the Raman spectra of benzenethiol adsorbed on two different substrates: a commercial Klarite SERS substrate and the BSC/Au NP core-shell substrates. Raman signals at 417, 691, 999, 1022, 1073, 1110 and 1573 cm^{-1}, originating from benzenethiol [17], were observed for the samples. An excellent correlation between the peak positions and the relative intensities of the two Raman spectra was observed for benzenethiol when adsorbed on the samples. The sensitivity increased remarkably from the commercial Klarite to the BSC/Au NP core-shell sphere substrate. The SERS signal intensity at 1075 cm^{-1} for the BSC/Au NP core-shell sphere substrate was about 10 times higher than that for the Klarite SERS substrate.

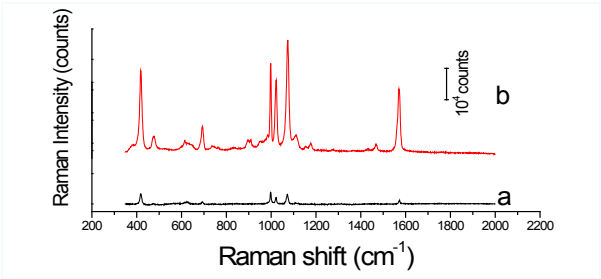

Figure 4: SERS spectra of benzenethiol adsorbed on (**a**) Klarite SERS substrate, (**b**) BSC/Au NP core-shell sphere substrate. The benzenethiol-loading concentration and time are 1 μM

To determine the detection limit of the BSC/Au NP core-shell structures, the SERS substrates were exposed overnight to benzenethiol solutions varying in concentration between 10^{-9}–10^{-6} M. Figure 5 shows the SERS spectra of these samples. As expected, the Raman signals of the benzenethiol decrease with decreasing benzenethiol-loading concentration. But the SERS peaks at 999, 1022, and 1110 cm^{-1} can be clearly observed down to a benzenethiol concentration of 1 nM.

It can be inferred that the following three factors mainly contribute to the high SERS intensity for the 3D BSC/Au NP core-shell structures. Firstly, it is well known that the SERS is proportional to the modulus of the localized electromagnetic field squared at the location of the analyte molecule. The interparticle coupling between the gold NPs on the surface of

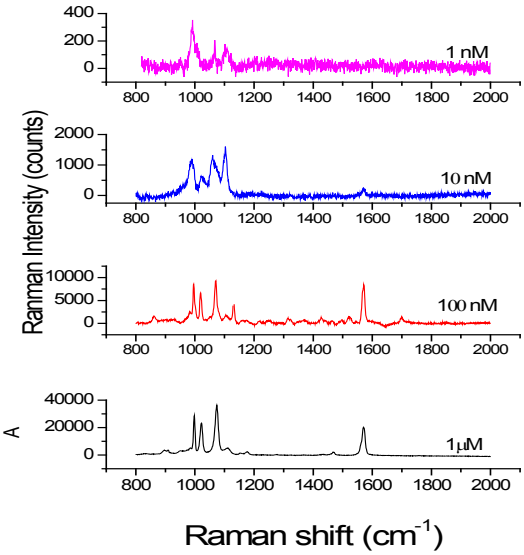

Figure 5: SERS spectra of benzenethiol adsorbed on BSC/Au NP core-shell spheres as a function of benzenethiol-loading concentration

the 3D BSC nanostructures may induce a strong electromagnetic field enhancement, resulting in the high SERS activity. Secondly, the 3D spherical feature of the BSC/Au NP core-shell structures preferably scatters more Raman photons into the detector than a flat substrate. Thirdly, the 3D BSC/Au NP core-shell structures tend to adsorb more analytes due to the large number of voids (i.e. hot spots) in the structures leading to the high SERS activity. Several advantages of the proposed method should be highlighted. First, this approach is a convenient method for the fabrication of SERS substrate with high yield and efficiency. The mesostructure of the 3D BSC provides ideal attachment sites for the nucleation and firm bonding of the metal NPs, as well as the adsorption of the analytes of interest. Second, the assembly of metal NPs onto the 3D BSC can be controlled by the deposition conditions including temperature, concentration, and deposition time, which makes it possible to realize the control of distribution, amount, size and composition of the metal NPs. Various metals, such as Au, Ag and alloys NPs have been successfully deposited on the 3D BSC nanostructures, and these studies are under way. BSC is a commonly used medication. The combination of treatment and detection functions of the BSC/Au NPs core-shell structures may pave the way towards the development of new biomedical devices.

Conclusions

In summary, we present a simple and effective method for morphogenesis and self-assembly of BSC nanocrystals into 3D nanostructures. The synergistic effect between hydroxide and citrate ions on the formation of BSC nano- and microcrystals and nanostructures has been explored and the formation mechanism of the 3 D nanostructures has been proposed. The SERS substrates based on 3 D BSC/gold nanoparticles core-shell spheres exhibit a high sensitivity with detection limit below 1 nM. The direct fabrication of 3D ternary hierarchical nanostructures may open up new opportunities to fabricate complex and functional superstructures and nanodevices.

Acknowledgment

This work was supported by the Australian Research Council (ARC) (Grant No.: DP120104334) and Monash University.

References

1. Zhang JZ. Acc. Chem. Res. 1997; 30:423.
2. Aguiló M, Woensdregt CFJ. Cryst. Growth. 1984; 69:527.
3. Lim B, Yu TY, Xia YN. Angew. Chem. Int. Ed. 2010; 49(51):9819-9820.
4. Tian ZR, Voigt JA, Liu J, Mc Kenzie J, Mc Dermott B, Rodriguez MJ, et al. Nat. Mater. 2003; 2:821.
5. Li F, Ding Y, Gao PX, Xin XQ, Wang ZL. Angew. Chem. Int. Ed. 2004; 43(39):5238.
6. Siegfried MJ, Choi KS. Angew. Chem. Int. Ed. 2008; 47:368.
7. Radi A, Pradhan D, Sohn YK, Leung KT. ACS Nano. 2012; 4(3):1553.
8. Miszta K, Graaf JD, Bertoni G, Dorfs D, Brescia R, Marras S, et al. Nature Mater.2011; 10:872.
9. Zhang ZP, Sun HP, Shao XQ, LiDF, Yu HD, Han MY. Adv. Mater. 2005; 17:42.
10. Briand GG, Burford N. Chem. Rev. 1999; 99:2601.
11. Zhao TY, Zai JT, Xu M, Zou Q, Su YZ, Wang KX, et al. Cryst Eng Comm. 2011; 13:4010.
12. Cao XF, Zhang L, Chen XT, Xue ZL. Cryst Eng Comm. 2011; 13:1935.
13. Dong F, Ho WK, Lee SC, Wu ZB, Fu M, Zou SC, et al. Mater. Chem. 2011; 21:12428.
14. Zhang Y, Duan F, Chen MQ, XieYJ. Mol. Catal. A. Chem. 2010; 317 (1-2): 34.
15. Chen R, So MH, Yang J, Deng F, Che CM, Sun HZ. Chem. Commun. 2006; 2265.
16. Cheng G, Yang HM, Rong KF, Lu Z, Yu XL, Chen RJ. Solid State Chem. 2010; 183:1878.
17. Joo TH, Kim MS, Kim KJ. Raman Spectrosc. 1987; 18:57.